The influence of negatively charged heavy ions on Alfven waves in a cometary environment

Sreekala G[1], Sijo Sebastian[1], Manesh Michael[1], Neethu Theresa Willington[1],

Noble P Abraham[1], G Renuka[2] and Chandu Venugopal[1,*]

[1]School of Pure & Applied Physics, Mahatma Gandhi University, Priyadarshini Hills, Kottayam – 686 560, Kerala, India.

* cvgmgphys@yahoo.co.in

[2]Kerala State Council for Science, Technology and Environment, Sasthra Bhavan, Pattom, Thiruvananthapuram – 695 004, Kerala, India.

ABSTRACT

Alfven waves are important in a wide variety of areas like astrophysical, space and laboratory plasmas. In cometary environments, waves in the hydromagnetic range of frequencies are excited predominantly by heavy ions. We, therefore, study the stability of Alfven waves in a plasma of hydrogen ions, positively and negatively charged oxygen ions and electrons. Each species has been modeled by drifting distributions in the direction parallel to the magnetic field; in the perpendicular direction the distribution is simulated with a loss cone type distribution obtained through the subtraction of two Maxwellian distributions with different temperatures. We find that for frequencies $\omega^* < \omega_{cH^+}$ (ω^* and ω_{cH^+} being respectively the Doppler shifted and hydrogen ion gyro-frequencies), the peak growth rate increases with increasing negatively charged oxygen ion densities. On the other hand, for frequencies $\omega^* < \omega_{cO^+}, \omega_{cO^-}$ (ω_{cO} being the oxygen ion gyro-frequencies) the region of wave growth increases with increasing negatively charged oxygen ion densities.

Indexing terms/Keywords

Alfven waves, stability, multi-ion, negative-ion cometary plasma

Academic Discipline And Sub-Disciplines

Physics; Plasma Physics

SUBJECT CLASSIFICATION

PACS : 52.35-g, 95.30Qd

Council for Innovative Research

INTRODUCTION

Hydromagnetic wave activity has been observed in distinct space environments: in the distant magnetotail [1], in the magnetosheath [2], upstream of the earth's [3] and other planets' bow shocks [4] and upstream of interplanetary shocks [5] especially near comets. Specifically, Alfvenic turbulence has been detected in the magnetic field [6,7] and in the electron distribution [8] at comet Giacobini-Ziner by the ICE spacecraft. Similar turbulence has also been detected by Giotto [9] and Vega [10] spacecrafts at comet Halley. In addition to these observations, Alfvenic turbulence has also been observed in the solar wind protons and alpha particles, where the fluctuations were not only seen in the plasma velocity as expected for simple Alfven waves, but also in the density and temperature as Giotto approached comet Halley [11].

Since the anticipation of Ip and Axford [12] on theoretical grounds, of low frequency hydromagnetic turbulence upstream of a comet, possible excitation mechanisms emphasizing proton (or heavier) ion beams with Maxwellian [13] or drifting [14] velocity distributions have been studied. While these studies were restricted to parallel propagation, oblique propagation has also been considered [15]. In particular, Gary and Sinha [16] studied the stability of electromagnetic waves, below the proton cyclotron frequency, propagating parallel or anti-parallel to a uniform magnetic field, while Brinca and Tsurutani [17] studied numerically the oblique behavior of low frequency electromagnetic waves excited by cometary new born ions. Later, Killen et al [18] studied the excitation of obliquely propagating magnetosonic waves using a distribution function that represented a ring beam in the parallel direction and a delta function in the perpendicular direction, while Cao et al [19] investigated the oblique behavior of left circularly polarized electromagnetic waves driven by a ring of gyrotropic ions, again modeled by delta function distributions. Thus in the analytical studies cited above, the thermal spreads of the particle distribution functions in the perpendicular directions were not considered. Besides, where applicable, these studies were confined to a plasma composition of hydrogen ions and electrons with only positively charged oxygen ions as the heavy ion component. However, negatively charged ions in three broad mass peaks of 7 – 19, 22 – 65 and 85 – 110 amu have also been observed in the coma of comet Halley. Of the many ionic components, negatively charged oxygen (O⁻) was unambiguously identified [20].

In general, a cometary environment contains hydrogen and new born heavier ions with relative densities depending on the distances from the nucleus, and each isolated beam capable of exciting instabilities. A model of the solar wind permeated by dilute, drifting ring distributions of electrons, hydrogen ions and positively charged oxygen ions with finite thermal spreads, was used to study numerically the electromagnetic waves excited by cometary new born ions [21]. In this model, the modes excited in the hydromagnetic frequency range were predominantly fed by the positively charged heavier oxygen ions.

We have therefore studied the stability of Alfven waves in a plasma of hydrogen ions, positively and negatively charged oxygen ions and electrons. It is found that for frequencies $\omega^* < \omega_{cH^+}$ (ω^* and ω_{cH^+} being respectively the Doppler shifted and the hydrogen ion-gyro frequencies), the growth rate increases with increasing negative oxygen ion densities. But, for frequencies $\omega^* < \omega_{cO^+}, \omega_{cO^-}$ (ω_{cO} being the oxygen ion gyro-frequencies) it is the region of wave growth that increases with increasing negatively charged oxygen ion densities.

THE ELEMENTS OF THE DIELECTRIC TENSOR

As mentioned above, we are interested in the stability of Alfven waves in a plasma of hydrogen ions (H+), positively and negatively charged oxygen ions (O+ and O- respectively) and electrons (e), with each species being modeled by drifting distributions in the direction parallel to the magnetic field and other ring, simulated by a loss-cone type distribution obtained through the subtraction of two Maxwellians with different temperatures . This distribution function is given by [21]

$F_s(v_\perp, v_\parallel) = f_{\perp s}(v_\perp) \, f_{\parallel s}(v_\parallel)$ where

$$f_{\parallel s}(v_\parallel) \;=\; \frac{1}{\sqrt{\pi} \; V_{ts}} \exp\left[-\left(\frac{v_\parallel \; - \; V_{sw} \; \cos\alpha}{V_{ts}} \right)^2 \right] \quad (1)$$

and

$$f_{\perp s}(v_\perp) \;=\; \frac{1}{\pi \, (a_s \; - \; b_s) \; V_{ts}^2} \left[\exp\left(-\frac{v_\perp^2}{a_s \, V_{ts}^2} \right) \; - \; \exp\left(-\frac{v_\perp^2}{b_s \, V_{ts}^2} \right) \right] a_s \; > \; b_s \quad (2)$$

In the above V_{sw} and V_{ts} are respectively the velocity of the solar wind and thermal velocity of species 's' (= H+, O+, O- or e); α is the pitch angle.

The elements of the dielectric tensor $D_{ij} (i, j = x, y, z)$ required for the derivation of the dispersion relation of Alfven waves are well known and hence will not be given here [22, 23].

We substitute (1) and (2) into these expressions and carry out the $dv_{\parallel}$ integrations using the plasma dispersion function [24]

$$Z(\zeta) = \frac{1}{\sqrt{\pi}} \int \frac{\exp(-x^2)}{x - \zeta} \, dx \quad (3)$$

and the $dv_{\perp}$ integrations using the basic form [25]

$$\int_0^{\infty} \exp(-x^2 / V_t^2) \, J_n(\alpha \, x) \, J_n(\beta \, x) \, x \, dx = \frac{V_t^2}{2} \exp\left[-\frac{(\alpha^2 + \beta^2) \, V_t^2}{4} \right] I_n\left(\frac{\alpha \, \beta \, V_t^2}{2}\right) = \frac{V_t^2}{2} \chi_n \quad (4)$$

The final expressions for the elements of the dielectric tensor are:

$$D_{xx} = 1 - \frac{c^2 \, k_{\parallel}^2}{\omega^2} + \sum_s \frac{\omega_{ps}^2}{\omega^2 \, (a_s - b_s)} \sum_n n^2 \left\{ \chi_n \left[\frac{\omega^*}{k_{\parallel} \, V_{ts}} Z(\zeta_s) - \left(1 + \zeta_s \, Z(\zeta_s)\right) \right] + \right.$$

$$\left. \phi_n \left(1 + \zeta_s \, Z(\zeta_s)\right) \right\} \quad (5)$$

$$D_{yy} = 1 - \frac{c^2 \, k^2}{\omega^2} - \sum_s \frac{\omega_{ps}^2}{\omega^2 \, (a_s - b_s)} \sum_n \left\{ \left(1 - \frac{n \, \omega_{cs}}{k_{\parallel} \, V_{ts}} Z(\zeta_s)\right) \left[a_s \, \psi_n(a_s \, L_{\perp s}) - b_s \, \psi_n(b_s \, L_{\perp s}) \right] - \right.$$

$$\left. \left(1 + \zeta_s \, Z(\zeta_s)\right) \left[a_s^2 \, \psi_n(a_s \, L_{\perp s}) - b_s^2 \, \psi_n(b_s \, L_{\perp s}) \right] \right\} \quad (6)$$

$$D_{xy} = -i \sum_s \frac{\omega_{ps}^2}{\omega^2 \, (a_s - b_s)} \sum_n n \left\{ \left(1 - \frac{n \, \omega_{cs}}{k_{\parallel} \, V_{ts}} Z(\zeta_s)\right) \left[a_s \, \eta_n(a_s \, L_{\perp s}) - b_s \, \eta_n(b_s \, L_{\perp s}) \right] - \right.$$

$$\left. \left(1 + \zeta_s \, Z(\zeta_s)\right) \left[a_s^2 \, \eta_n(a_s \, L_{\perp s}) - b_s^2 \, \eta_n(b_s \, L_{\perp s}) \right] \right\} \quad (7)$$

$$D_{xz} = \frac{c^2 \, k_{\parallel} \, k_{\perp}}{\omega^2} + \frac{k_{\perp}}{k_{\parallel}} \sum_s \frac{\omega_{ps}^2}{\omega^2 (a_s - b_s)} \sum_n \left\{ n^2 \, \chi_n \left[1 + \left(\zeta_s + \frac{V_{sw} \cos \alpha}{V_{ts}}\right) Z(\zeta_s)\right] + \right.$$

$$\left. \frac{n \left(\omega - n \, \omega_{cs}\right)}{\omega_{cs}} \phi_n \left(1 + \zeta_s \, Z(\zeta_s)\right) \right\} \quad (8)$$

$$D_{zx} = \frac{c^2 \, k_{\parallel} \, k_{\perp}}{\omega^2} + \sum_s \frac{\omega_{ps}^2}{\omega^2 (a_s - b_s)} \sum_n \left\{ \frac{k_{\perp}}{k_{\parallel}} \, \frac{\omega}{\omega_{cs}} \, n \, \chi_n \left[1 + \zeta_s \, Z(\zeta_s) + \frac{V_{sw} \cos \alpha}{V_{ts}} Z(\zeta_s) \right] \right.$$

$$- \frac{k_\perp V_{ts}}{\omega_{cs}} \ n \ \chi_n \ [\ \Big(1 \ + \ \zeta_s \ Z(\zeta_s)\Big)\Big(\zeta_s \ + \ 2 \ \frac{V_{sw}\cos\alpha}{V_{ts}}\Big) \ + \ \Big(\frac{V_{sw}\cos\alpha}{V_{ts}}\Big)^2 \ Z(\zeta_s) \ ] \ +$$

$$\frac{n \ \omega_{cs}}{k_\perp \ V_{ts}} \Big(\frac{\omega \ - \ n \ \omega_{cs}}{k_\parallel \ V_{ts}}\Big) L_{\perp s} \ \phi_n \ \Big(1 \ + \ \zeta_s \ Z(\zeta_s)\Big) \ \} \quad (9)$$

$$D_{zy} \ = \ -i \ \sum_s \frac{\omega_{ps}^2}{\omega^2 \ (a_s \ - \ b_s)} \frac{k_\perp}{\omega_{cs}} \sum_n \ \{ \ [\ V_{sw} \ \cos \ \alpha \ - \ \frac{n \ \omega_{cs}}{k_\parallel}\Big(1 \ + \ \frac{\omega \ - \ n \ \omega_{cs}}{k_\parallel \ V_{ts}} \ Z(\zeta_s)\Big)] \times$$

$$[\ a_s \ \eta_n(a_s \ L_{\perp s}) \ - \ b_s \ \eta_n(b_s \ L_{\perp s}) \ ] \ -$$

$$\Big(\frac{\omega \ - \ n \ \omega_{cs}}{k_\parallel}\Big)\Big(1 \ + \ \zeta_s \ Z(\zeta_s)\Big) [\ a_s^2 \ \eta_n(a_s \ L_{\perp s}) \ - \ b_s^2 \ \eta_n(b_s \ L_{\perp s}) \ ] \quad (10)$$

$$D_{yz} \ = \ -i \ \sum_s \frac{\omega_{ps}^2}{\omega^2 \ (a_s \ - \ b_s)} \frac{k_\perp}{k_\parallel} \sum_n \ \{ \ \Big(\frac{\omega \ - \ n \ \omega_{cs}}{\omega_{cs}}\Big) \Big(1 \ + \ \zeta_s \ Z(\zeta_s)\Big) \times$$

$$[\ a_s^2 \ \eta_n(a_s \ L_{\perp s}) \ - \ b_s^2 \ \eta_n(b_s \ L_{\perp s}) \ ] \ +$$

$$n \ \Big(1 \ + \ \frac{\omega \ - \ n \ \omega_{cs}}{k_\parallel \ V_{ts}} \ Z(\zeta_s)\Big) [\ a_s \ \eta_n(a_s \ L_{\perp s}) \ - \ b_s \ \eta_n(b_s \ L_{\perp s}) \ ] \ \} \quad (11)$$

$$D_{zz} \ = \ 1 \ - \ \frac{c^2 \ k_\perp^2}{\omega^2} \ + \ 2 \ \sum_s \frac{\omega_{ps}^2}{\omega^2(a_s \ - \ b_s)} \sum_n \ \{ \ \frac{n \ \omega_{cs}}{k_\parallel \ V_{ts}} \ L_{\perp s} \ \chi_n \ [\ \Big(1 \ + \ \zeta_s \ Z(\zeta_s)\Big)\Big(\zeta_s \ + \ 2 \ \frac{V_{sw}\cos\alpha}{V_{ts}}\Big)$$

$$+ \ \Big(\frac{V_{sw}\cos\alpha}{V_{ts}}\Big)^2 \ Z(\zeta_s) \ ] \ + \ \Big(\frac{\omega \ - \ n \ \omega_{cs}}{k_\parallel \ V_{ts}}\Big)^2 \ L_{\perp s} \ \phi_n \ \Big(1 \ + \ \zeta_s \ Z(\zeta_s)\Big) \ \} \quad (12)$$

where

$$L_{\perp s} \ = \ k_\perp^2 \ V_{ts}^2 \ /(2 \ \omega_{cs}^2)$$

$$\Lambda_n(a_s L_{\perp s}) \ = \ \exp(-a_s L_{\perp s}) \ I_n(a_s L_{\perp s})$$

$$\eta_n(a_s L_{\perp s}) \ = \ \exp(-a_s L_{\perp s}) \ [\ I_n'(a_s L_{\perp s}) \ - \ I_n(a_s L_{\perp s}) \ ]$$

$$\psi_n(a_s L_{\perp s}) \ = \ \exp(-a_s L_{\perp s})[\ a_s \ L_{\perp s} \ I_n(a_s L_{\perp s}) \ + \ (1 \ - \ 2 \ a_s L_{\perp s}) \ I_n'(a_s L_{\perp s}) \ + \ a_s \ L_{\perp s} \ I_n''(a_s L_{\perp s}) \ ] \quad (13)$$

with

$$\chi_n \ = \ \frac{\Lambda_n(a_s \ L_{\perp s}) \ - \ \Lambda_n(b_s \ L_{\perp s})}{L_{\perp s}} \quad (14 \ a)$$

and

$$\varphi_n = \frac{a_s \, \Lambda_n(a_s \, L_{\perp s}) \; - \; b_s \, \Lambda_n(b_s \, L_{\perp s})}{L_{\perp s}} \qquad (14\ b)$$

In the above, 's' indicates a summation over the species (= H, O$^+$, O$^-$ or e), $\omega_{ps} = (4\ \pi\ n_{0s}\ e^2\ /\ m_s)^{1/2}$ is the corresponding plasma frequency while $\omega_{cs} = |e|\ B_0\ /\ (m_s\ c)$ is the gyro-frequency; $k_\perp$ and $k_\parallel$ are respectively the wave vectors perpendicular and parallel to the magnetic field. Also I$_n$ are the modified Bessel functions of order n. The argument ζ_s of the dispersion function $Z(\zeta_s)$ is

$$\zeta_s = \frac{\omega \; - \; k_\parallel \, V_{sw} \cos \; - \; n\ \omega_{cs}}{k_\parallel \, V_{ts}} = \frac{\omega^* \; - \; n\ \omega_{cs}}{k_\parallel \, V_{ts}} \qquad (15)$$

THE DISPERSION FORMULA

The elements $D_{i\ j}(i,\ j\ =\ x,\ y,\ z)$ can be used to form the dielectric tensor, which is given by

$$\begin{vmatrix} D_{xx} & D_{xy} & D_{xz} \\ D_{yx} & D_{yy} & D_{yz} \\ D_{zx} & D_{zy} & D_{zz} \end{vmatrix} = 0 \ (16)$$

Expanding (16) by the last row, dividing and multiplying throughout respectively by D$_{zz}$ and $\left(\omega^2\ /\ \omega_{pH}^2\right)^2$, we get

$$\left[D_{xx}\left[\frac{\omega^2}{\omega_{pH}^2}\right] D_{yy}\left[\frac{\omega^2}{\omega_{pH}^2}\right] - D_{xy}\left[\frac{\omega^2}{\omega_{pH}^2}\right] D_{yx}\left[\frac{\omega^2}{\omega_{pH}^2}\right] \right] -$$

$$\frac{D_{zy}\left[\frac{\omega^2}{\omega_{pH}^2}\right]}{D_{zz}\left[\frac{\omega^2}{\omega_{pe}^2}\right]\left[\frac{\omega_{pe}^2}{\omega_{pH}^2}\right]} \left[D_{xx}\left[\frac{\omega^2}{\omega_{pH}^2}\right] D_{yz}\left[\frac{\omega^2}{\omega_{pH}^2}\right] - D_{yx}\left[\frac{\omega^2}{\omega_{pH}^2}\right] D_{xz}\left[\frac{\omega^2}{\omega_{pH}^2}\right] \right] +$$

$$\frac{D_{xz}\left[\frac{\omega^2}{\omega_{pH}^2}\right]}{D_{zz}\left[\frac{\omega^2}{\omega_{pe}^2}\right]\left[\frac{\omega_{pe}^2}{\omega_{pH}^2}\right]} \left[D_{xy}\left[\frac{\omega^2}{\omega_{pH}^2}\right] D_{yz}\left[\frac{\omega^2}{\omega_{pH}^2}\right] - D_{yy}\left[\frac{\omega^2}{\omega_{pH}^2}\right] D_{xz}\left[\frac{\omega^2}{\omega_{pH}^2}\right] \right] = 0 \qquad (17)$$

Equation (17) is the dispersion formula that will be used in the derivation of the dispersion relations.

Expressions for the tensor elements

We now derive explicit expressions for the elements of the dielectric tensor. We use the asymptotic expansion for the plasma dispersion function which is given by $Z(\zeta_s) = -\frac{1}{\zeta_s} - \frac{1}{2\ \zeta_s^3} - ... + i\ \sqrt{\pi}\ \exp(-\zeta_s^2)$ [24]. The exponential term and the modified Bessel functions in (13) and (14) were expanded as a power series and terms of the order of $L_\perp^2$ and above were neglected. The contributions were as follows: $n\ =\pm 1$ ion terms to D_{xx}; n = 0 electron and ion terms and $n\ =\pm 1$ ion terms to D_{yy}; $n\ =\pm 1$ electron and ion terms to D_{xy}; $n\ =\pm 1$ ion terms to D_{xz}; n = 0 electron and

ion terms and $n = \pm 1$ ion terms to D_{zy}; $n = \pm 1$ ion terms to D_{yz} and the n = 0 electron terms to D_{zz}. The simplified final expressions for the tensor elements are:

$$D_{xx} = 1 - \frac{c^2 k_{\parallel}^2}{\omega^2} - \frac{1}{\omega^2} \sum_j \omega_{p\,j}^2 \left[1 - \left(a_s - b_s \right) L_{\perp j} \right] \left[\frac{\omega^{*2}}{\omega^{*2} - \omega_{c\,j}^2} \right]$$

$$D_{yy} = 1 - \frac{c^2 (k_{\parallel}^2 + k_{\perp}^2)}{\omega^2} - \frac{1}{\omega^2} \left\{ 2\, \omega_{pe}^2\, L_{\perp_e} \left[(a_s + b_s) - i\, \sqrt{\pi}\, e^{-\zeta_{0e}^2} \frac{\omega^*}{k_{\parallel}\, V_{te}} \left(a_s^2 + a_s\, b_s + b_s^2 \right) \right] \right.$$

$$\left. + \sum_j \omega_{p\,j}^2 \left(2\, L_{\perp j} \left(a_s + b_s \right) + \left[1 - 3\, L_{\perp j} \left(a_s + b_s \right) \right] \left[\frac{\omega^{*2}}{\omega^{*2} - \omega_{c\,j}^2} \right] \right) \right\}$$

$$D_{xy} = - \frac{i}{\omega^2} \sum_j \omega_{p\,j}^2\, \omega_{c\,j} \left[\frac{\omega^*}{\omega^{*2} - \omega_{c\,j}^2} \right] \left[1 - 2 \left(a_s + b_s \right) L_{\perp\,j} \right]$$

$$D_{xz} = \frac{c^2 k_{\parallel} k_{\perp}}{\omega^2} - \frac{2\, V_{sw}\, \omega^*\, \cos\alpha}{\omega^2\, k_{\perp}} \sum_j \frac{\omega_{p\,j}^2}{V_{t\,j}^2} L_{\perp j} \left[\frac{\omega_{c\,j}^2}{\omega^{*2} - \omega_{c\,j}^2} \right]$$

$$D_{yz} = \frac{i\, k_{\perp}\, V_{sw}\, \cos\alpha}{\omega^2} \sum_j \omega_{p\,j}^2 \left[\frac{\omega_{c\,j}}{\omega^{*2} - \omega_{c\,j}^2} \right] \left[1 - 2 \left(a_s + b_s \right) L_{\perp j} \right]$$

$$D_{zy} = - \frac{i\, k_{\perp}\, V_{sw}\, \cos\alpha}{\omega^2} \left\{ - \frac{\omega_{p\,e}^2}{\omega_{c\,e}} + \sum_j \frac{\omega_{p\,j}^2}{\omega_{c\,j}} \left\{ \left[\frac{3\,(a_s + b_s)}{2} L_{\perp j} - 1 \right] + \left[1 - 2(a_s + b_s) L_{\perp j} \right] \right. \right.$$

$$\left. \left. \left[\frac{\omega^{*2}}{\omega^{*2} - \omega_{cj}^2} \right] \right\} \right\}$$

$$D_{zz} = - \frac{c^2 k_{\perp}^2}{\omega^2} - \frac{\omega_{p\,e}^2}{\omega^{*2}} + 2\, i\, \omega_{pe}^2\, \sqrt{\pi}\, e^{-\zeta_{0e}^2} \frac{\omega^*}{k_{\parallel}^3\, V_{te}^3} \quad (18)$$

In expressions (18), j = H, O+ or O-. Also $D_{xz} = D_{zx}$ and $D_{xy} = -D_{yx}$

RESULTS

Waves in the frequency range ω_{cO^+} , $\omega_{cO^-} \ll \omega^* \ll \omega_{cH^+}$

In this subsection we consider the stability of Alfven waves in the frequency range ω_{cO^+}, $\omega_{cO^-} \ll \omega^* \ll \omega_{cH^+}$. The tensor elements (18) were re-derived for this frequency range; they were then substituted into the dispersion formula (17)

which was then solved for typical parameters observed around comet Halley. These parameters are [11, 20, 21]: n_{H^+} = 6.4 cm^{-3}, n_{O^+} = 0.5 cm^{-3}, T_e = 1× 10^6 K, T_{H^+} = 9 × 10^5 K, V_{sw} = $400\ km\ s^{-1}$, T_{O^+} = T_{O^-} = 1.2 × 10^3 K and B$_0$ = 0.6 g. The stability of the waves were studied as a function of the propagation angle θ , the density of negatively charged oxygen ions n_{O^-} and the parameters a$_s$ and b$_s$ that describe the distribution functions.

Figure 1
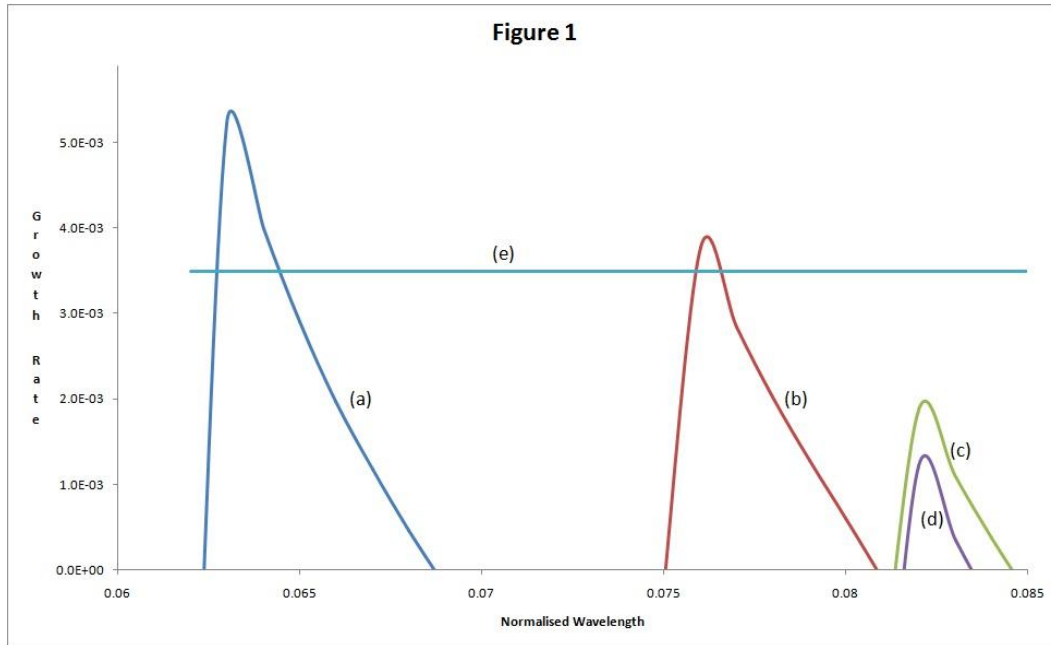
Fig. 1: Plot of the normalized growth rate (with respect to ω_{cH^+}) versus $k_\perp\ r_{LH^+}$ in the frequency range

$$\omega_{cO^+}, \omega_{cO^-} << \omega^* << \omega_{cH^+} \text{ for } n_{H^+} = 6.4\,\text{cm}^{-3}, a_s = 1.8, b_s = 1.2, n_{O^+} = 0.5\ \text{cm}^{-3}, n_{O^-} = 0.4\ \text{cm}^{-3}$$

$$T_e = 1 \times 10^6\ {}^oK, \quad T_{H^+} = 9 \times 10^5\ {}^oK \text{ and } T_{O^+} = T_{O^-} = 1.2 \times 10^3\ {}^oK \text{ as a function of the propagation angle.}$$

Curve (a) is for a propagation angle θ =1^0, curve (b) for θ = 2^0, curve (c) for θ = 5^0, curve (d) for θ = 9^0 while curve (e) is for parallel propagation. It may be noted that the values for curve (e) have been divided by 10 to fit into the figure.

Figure 1 is a plot of the growth rate (all growth rates have been normalized with respect to ω_{cH^+}) versus normalized wave number $k_\perp\ r_{LH^+}$ as a function of the propagation angle θ, for n_{H^+} = 6.4 cm^{-3}, n_{O+} = 0.5 cm^{-3}, n_{O^-} = 0.4 cm^{-3}, T_e = 1 × 10^6 K, T_{H^+} = 9 × 10^5 K, T_{O^+} = T_{O^-} = 1.2 × 10^3 K , b$_s$ = 1.2 and a$_s$ = 1.5 b$_s$. Curve (a) is for a propagation angle θ =1^0, curve (b) for θ = 2^0, curve (c) for θ = 5^0, curve (d) for θ = 9^0 while curve (e) is for parallel propagation. It may be noted that the values for curve (e) have been divided by 10 to fit into the figure. Thus the growth rate is a maximum for θ = 0^0. For near parallel angles, as can be seen from the figure, the wave growth decreases both in magnitude as well as wave number range. The shift towards higher wave numbers with increasing θ does not occur indefinitely; beyond 5^0 the region of wave growth occurs within the wave number region of 5^0 and also decreases rapidly.

We study the stability of the wave as a function of the negative oxygen ion density in figure 2. Thus the growth rate has been plotted against normalized wave number $k_\perp\ r_{LH^+}$ for n_{H^+} = 6.4 cm^{-3}, n_{O+} = 0.5 cm^{-3} as a function of n_{O^-} ; the propagation angle θ = 1^0 while the other parameters are the same as in figure 1. Curve (a) is for $n_{O^-} = 0$, curve (b) for $n_{O^-} = 0.2$ cm^{-3} and curve (c) for $n_{O^-} = 0.4$ cm^{-3}. We find that the growth rate increases with increasing n_{O^-} density.
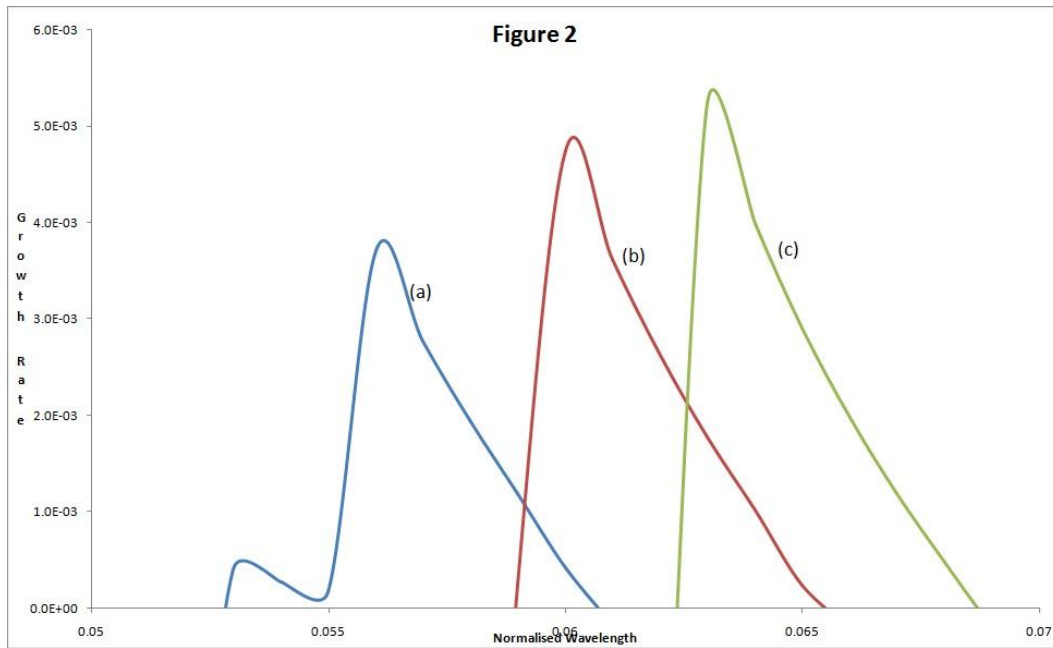
Figure 2

Fig. 2: Plot of the normalized growth rate (with respect to ω_{cH^+}) versus $k_\perp \, r_{LH^+}$ in the frequency range $\omega_{cO^+}, \quad \omega_{cO^-} << \omega^* << \omega_{cH^+}$ as a function of the negatively charged oxygen density for a propagation angle of θ = 1^0. Curve (a) is for $n_{O^-} = 0$, curve (b) is for $n_{O^-} = 0.2$ cm^{-3} and curve (c) for $n_{O^-} = 0.4$ cm^{-3}, the other parameters are the same as in figure 1.
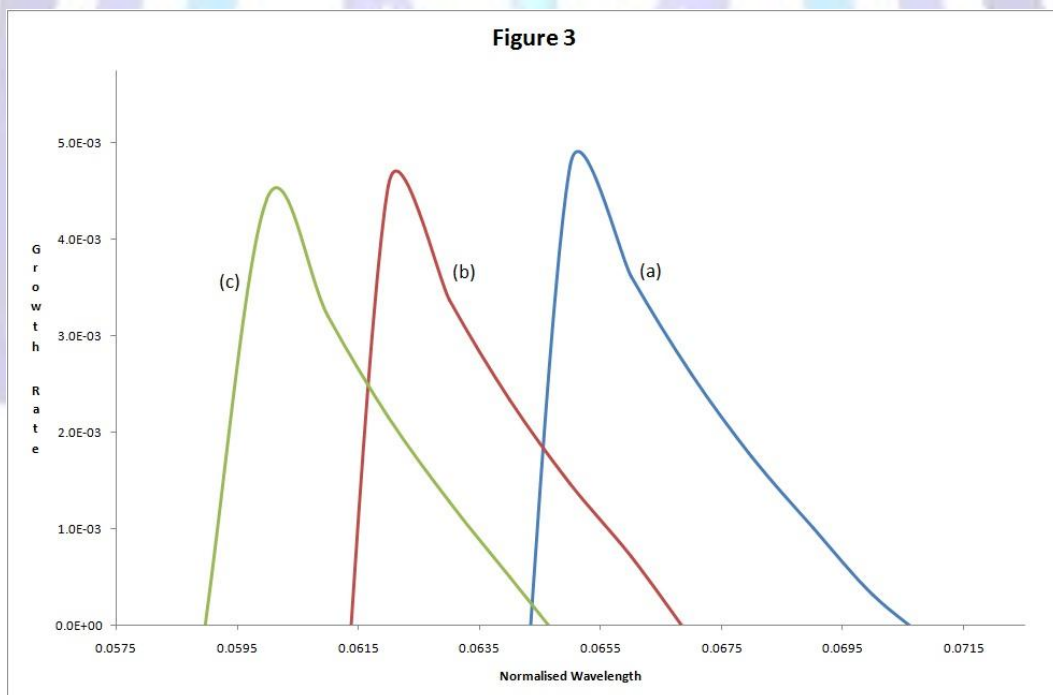
Figure 3

Fig. 3: Plot of the normalized growth rate (with respect to ω_{cH^+}) versus $k_\perp \, r_{LH^+}$ in the frequency range $\omega_{cO^+} , \omega_{cO^-} << \omega^* << \omega_{cH^+}$ as a function of the parameter b_s, the densities being n_{H^+} = 6.4 cm^{-3}, n_{O_+}

= 0.5 cm^{-3}, n_{O-} = 0.4 cm^{-3} and propagation angle θ =1^0 . The temperatures remain unchanged from the previous figures. Curve (a) is for b$_s$ = 1.3, curve (b) for b$_s$ = 1.7 and curve (c) for b$_s$ = 2.0 , with $a_s = 1.5 \, b_s$.

The perpendicular component of the distribution function $f_{\perp s}(v_\perp)$ in (2) reduces to a Maxwellian distribution when b$_s$ = 0; for b$_s$ ≠ 0, (2) simulates a loss cone distribution. It would thus be interesting to study the effect of b$_s$ on the stability of the Alfven wave. Figure (3) is thus a plot of the growth rate versus the normalized wave number $k_\perp \, r_{LH^+}$ as a function of b$_s$, the parameters being n_{H^+} = 6.4 cm^{-3}, n_{O+} = 0.5 cm^{-3}, n_{O-} = 0.4 cm^{-3}, propagation angle θ =1^0, while the temperatures remain unchanged from the previous figures. Curve (a) is for b$_s$ = 1.3, curve (b) for b$_s$ = 1.7 and curve (c) for b$_s$ = 2.0 with $a_s = 1.5 \, b_s$. As is evident from the figure the wave growth region shifts towards lower $k_\perp \, r_{LH^+}$ as b$_s$ increases.

Waves in the frequency range $\omega^* << \omega_{cO^+} \, , \, \omega_{cO^-}$

In this subsection we consider of waves of frequency $\omega^* << \omega_{cO^+}, \omega_{cO^-}$ (and hence $\omega^* << \omega_{cH^+}$ also); the waves are thus of extremely low frequency. The tensor elements (18) were rederived in this frequency regime, substituted into the dispersion formula (17) and solutions obtained for the same parameters as in the previous subsection.
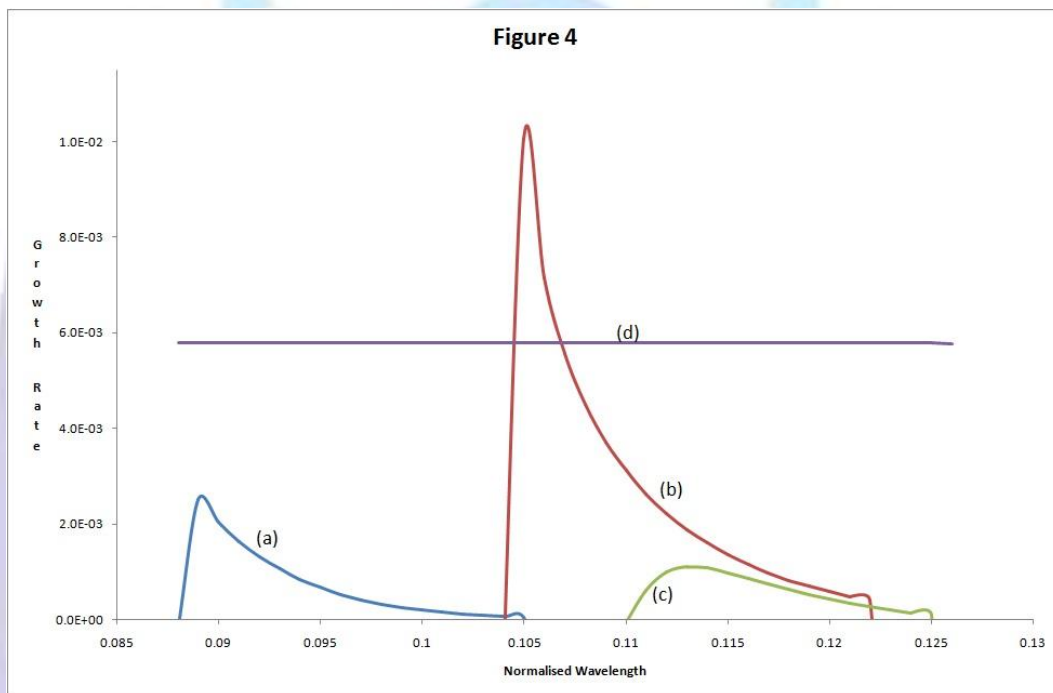

Fig. 4: Plot of the normalized growth rate (with respect to ω_{cH^+}) versus $k_\perp \, r_{LH^+}$ in the frequency range $\omega << \omega_{cO^+}, \omega_{cO^-}$ for $n_{H^+} = 6.4 \, \text{cm}^{-3}, a_s = 1.8, b_s = 1.2, n_{O^+} = 0.5$ cm^{-3}, $n_{O^-} = 0.4$ cm^{-3}, $T_e = 1 \times 10^6 \; ^oK,$ $T_{H^+} = 9 \times 10^5 \; ^oK$ and $T_{O^+} = T_{O^-} = 1.2 \times 10^3 \; ^oK$ as a function of the propagation angle. Curve (a) is for a propagation angle θ =1^0, curve (b) for θ = 6^0, curve (c) for θ = 8^0 while curve (d) is for parallel propagation. It may be noted that the values for curve (d) have been divided by 10.

Figure (4) is a plot of the growth rate versus $k_\perp \, r_{LH^+}$ as a function of the propagation angle θ, the species densities being n_{H^+} = 6.4 cm^{-3}, n_{O+} = 0.5 cm^{-3}, n_{O-} = 0.4 cm^{-3}, b$_s$ = 1.2, a$_s$ = 1.5 b$_s$; the temperatures remaining unchanged. Curve (a) is for θ =1^0, curve (b) for θ = 6^0, curve (c) for θ = 8^0 while curve (d) is for θ = 0^0. As in figure 1, the values of curve (d) were divided by 10. The maximum growth rate is again for parallel propagation. However, for oblique propagation, the growth rates are small for low values of propagation angles (θ =1^0), they reach a maximum for θ = 6^0 and decrease thereafter.

The variation of the growth rate was also studied as a function of the n_{O-} density. Figure (5) is a plot of the growth rate versus $k_\perp r_{LH^+}$ with the propagation angle $\theta = 5^0$, $b_s = 1.2$, $a_s = 1.5\ b_s$; the temperatures again remaining unchanged. Curve (a) is for $n_{O^-} = 0$, curve (b) is for $n_{O^-} = 0.2$ cm^{-3} and curve (c) for $n_{O^-} = 0.4$ cm^{-3}. We find that the range of wave growth increases with increasing n_{O-} density.
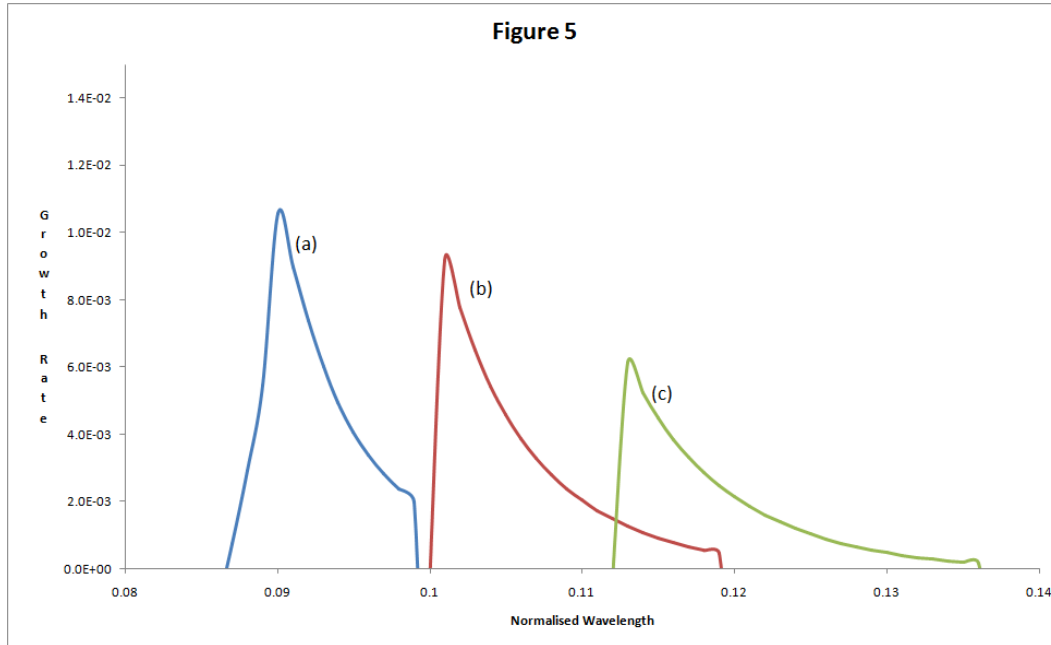

Figure 5

Fig. 5: Plot of the normalized growth rate (with respect to ω_{cH^+}) versus $k_\perp r_{LH^+}$ in the frequency range $\omega \ll \omega_{cO^+}, \omega_{cO^-}$ as a function of the negatively charged oxygen density for a propagation angle of $\theta = 5^0$. Curve (a) is for $n_{O^-} = 0$, curve (b) for $n_{O^-} = 0.2$ cm^{-3} and curve (c) for $n_{O^-} = 0.4$ cm^{-3}, the other parameters are the same as in figure 4.

Finally, the variation in the growth rate with the parameters a_s and b_s were similar to that in figure 3.

DISCUSSION

New born heavier ions picked up by the solar wind are generally believed responsible for hydromagnetic turbulence observed around comets. Of the many heavy ions, one that has been studied extensively has been opositively charged oxygen [21].

The mechanism of the instability has been envisioned as follows: the new born ions are picked into cycloidal orbits which combines gyration along with a drift perpendicular to the magnetic field. In the frame of reference moving with the solar wind, the ions are gyrating and also moving sunward along the magnetic field. This motion, parallel to the magnetic field, is believed to be the source of free energy ultimately responsible for the observed hydromagnetic turbulence [26].

The results of our study are generally supportive of this mechanism. Specifically, in figure 1 we have a situation where the growth rate is a maximum for parallel propagation and falls off rapidly with increasing angles of propagation. Figure 2, where the growth rate increases with increasing negative oxygen ion densities, also endorses the proposed mechanism since the free energy available increases with increasing n_{O-} densities.

As mentioned above, the particle distribution function perpendicular to the magnetic field simulates a loss cone distribution for $b_s \neq 0$. Thus increasing b_s makes available fewer particles as a source of free energy . This would explain the slight decrease in the growth rate of the wave as b_s increases (for waves in the frequency range $\omega_{cO^+}, \omega_{cO^-} \ll \omega^* \ll \omega_{cH^+}$ (figure 3) and similarly for waves in the frequency range $\omega^* \ll \omega_{cO^+}, \omega_{cO^-}$; not shown).

We next consider waves in the frequency range $\omega^* \ll \omega_{cO^+}, \omega_{cO^-}$. As in figure 1, the growth rate is again a maximum for parallel propagation. However, unlike the case of figure 1, there is a secondary maximum at oblique propagation. This

could be due to the fact that we are now dealing with lower frequency waves and have two ions of the same mass which could effectively interact with the wave.

Finally, in figure 5, though the peak growth decreases slightly with increasing n_{O^-}, the range of the instability increases and hence the explanation given in connection with figure 2 would be applicable here too.

CONCLUSIONS

We have, in this paper, studied the stability of the Alfven wave in a plasma composed of hydrogen ions, positively and negatively charged oxygen ions and electrons. All species of particles were modeled by distribution functions that could be separated into a drifting Maxwellian distribution in the direction parallel to the magnetic field; in the perpendicular direction the distribution function is of the loss-cone type obtained by subtracting two Maxwellian distributions. The peak value of the growth rate increases with increasing n_{O^-} for higher frequencies ; while for low frequencies , the growth region increases with increasing n_{O^-} .

ACKNOWLEDGMENTS

REFERENCES

[1] Tsurutani, B. T. and Smith, E. J. 1984. Magnetosonic Waves Adjacent To The Plasma Sheet In The Distant Magnetotail - ISEE-3 Geophys. Res. Lett. 11, 331-334

[2] Anderson, R. R., Harvey, C. C., M M Hoppe, B T Tsurutani, T E Eastman, and J J Etcheto, 1982. Plasma waves near the magnetopause, J. Geophys. Res. 87, 2087-2107

[3] Hoppe, M. M., Russel, C. T., Frank, L. A., Eastman, T. E. and Greenstadt, E, W., 1981. Upstream hydromagnetic waves and their association with backstreaming ion populations: ISEE 1 and 2 observations, J. Geophys. Res. 86, 4471-4492

[4] Smith, C. W. and Lee, M. A., 1986. Coupled hydromagnetic wave excitation and ion acceleration upstream of the Jovian bow shock, J. Geophys. Res. 91, 81-90

[5] Tsurutani, B. T., Smith, E. J. and Jones, D. E., 1983. Waves observed upstream of interplanetary shocks, J. Geophys. Res. 88, 5645-5656

[6] Tsurutani, B. T. and Smith, E. J., 1986. Strong hydromagnetic turbulence associated with comet Giacobini-Zinner, Geophys. Res. Lett. 13, 259-262

[7] Tsurutani, B. T. and Smith, E. J., 1986. Hydromagnetic waves and instabilities associated with cometary ion pickup: ICE observations, Geophys. Res. Lett. 13 263-266

[8] Gosling, J. T., Asbridge, J, R., Bame, S. J., Thomsen, M. F. and Zwickl, R. D., 1986. Large amplitude, low frequency plasma fluctuations at comet Giacobini-Zinner, Geophys. Res. Lett. 13, 267-270

[9] Neubauer, F. M., Glessmeier, K. H., Pohl, M., et al., 1986. First results from the Giotto magnetometer experiment at comet Halley, Nature 321, 352-354

[10] Reidler, W., Schwingenschuh, K., Yeroshenko, Y. G., Styashkin, V. A. and Russel, C, T., 1986. Magnetic field observations in comet Halley's coma, Nature 321, 288-289

[11] Johnstone, A. D., Glassmeier, K. H., and Acuna, M., 1987. Waves in the magnetic field and solar wind flow outside the bow shock at comet P/Halley, Astron. Astrophys. 187, 47-54

[12] Ip, W. H. and Axford, W, I., 1982. *Comets* ed Wilkening L L, p 588 Univ. Arizona Press Tuscon, Arizona.

[13] Gary, S. P., Madland, C. D. and Tsurutani, B. T., 1985. Electromagnetic ion beam instabilities: II, Phys. Fluids 28, 3691-3695

[14] Winske, D., Wu, C. S., Li, Y. Y., Mou, Z. Z. and Guo, S. Y. 1985. Coupling of newborn ions to the solar wind by electromagnetic instabilities and their interaction with the bow shock, J. Geophys. Res. 90 2713-2726

[15] Sharma, O. P. and Patel, V. L., 1986. Low-frequency electromagnetic waves driven by gyrotropic gyrating ion beams, J. Geophys. Res. 91, 1529-1534

[16] Gary, S. P. and Sinha, R., 1989. Electromagnetic waves and instabilities from cometary ion velocity shell distributions, J. Geophys. Res. 94, 9131-9138

[17] Brinca, A. L. and Tsurutani, B. T., 1989. The oblique behavior of low-frequency electromagnetic waves excited by newborn cometary ions, J. Geophys. Res. 94, 3-14

[18] Killen, K., Omidi, N., Krauss-Varban, D. and Karimabadi, H. 1995. Linear and nonlinear properties of ULF waves driven by ring-beam distribution functions, J. Geophys. Res. 100, 5835-5852

[19] Cao, J. B., Mazelle, C., Belmont, G. and Reme, H., 1998. Oblique ring instability driven by nongyrotropic ions: Application to observations at comet Grigg-Skjellerup, J. Geophys. Res. 103, 2055-2067

[20] Chaizy, P., Reme, H., Sauvaud, J. A., et. al., 1991. Negative ions in the coma of comet Halley, Nature 349, 393-396

[21] Brinca, A. L. and Tsurutani, B. T., 1987, Unusual characteristics of electromagnetic waves excited by cometary newborn ions with large perpendicular energies, Astron. Astrophys. 187, 311-319

[22] Galeev, A. A. and Sudan, R. N. (Ed) 1989. *Basic Plasma Physics* p 238 North Holland Publishers, Amsterdam.

[23] Krall, N. A. and Trivelpiece, A. W., 1973. *Principles of Plasma Physics*, p 349 San Francisco Press, San Francisco.

[24] Fried B. D. and Conte, S, D. 1961. *The Plasma Dispersion Function*, Academic Press, New York.

[25] Gradshteyn, I, S. and Ryzhik, I. M., 2007. *Tables of Integrals, Series and Products* p 707 Elsevier, Amsterdam.

[26] Johnstone, A. D., Coates, A. J., Heath, J., et. al., 1987. Alfvenic Turbulence in the Solar Wind Flow during the Approach to Comet p/ Halley, Astron. Astrophys. 187, 25-32